Antitumor potential of S-nitrosothiol-containing polymeric nanoparticles against melanoma

Original Article

Antitumor potential of S-nitrosothiol-containing polymeric nanoparticles against melanoma

Letícia S. Ferraz[1], Carolina M. Watashi[1], Carina Colturato-Kido[1], Milena T. Pelegrino[1], Edgar J. Paredes-Gamero[2], Richard B. Weller[3], Amedea B. Seabra[1,4], Tiago Rodrigues[1,4]*.

[1]Center for Natural and Human Sciences (CCNH), Federal University of ABC (UFABC), Santo André, SP, Brazil. [2]Interdisciplinary Center for Biochemistry Investigation (CIIB), University of Mogi das Cruzes (UMC), Mogi das Cruzes, SP, Brazil. [3]Medical Research Council Centre for Inflammation Research, University of Edinburgh, Queen's Medical Research Institute, Edinburgh, UK. [4]Nanomedicine Research Unit (NANOMED), Federal University of ABC (UFABC), Santo André, SP, Brazil.

Keywords: Cytotoxicity, Melanoma, Nanoparticles, Nitric Oxide, S-nitrosothiol.

This work was supported by the Brazilian funding agencies FAPESP (2012/12247-8; 2016/07367-5) and CNPq (486760/2013-0).

***Corresponding author:** Prof. Tiago Rodrigues, Ph.D. Center for Natural and Human Sciences, Federal University of ABC, UFABC. Avenida dos Estados, 5001. Bloco A, Torre 3, Sala 623, Santo André, SP, Brasil. CEP 090210-580. Santo André, SP. Brasil. e-mail: tiago.rodrigues@ufabc.edu.br.

All authors state no conflicts of interest.

Word count: Abstract: 142/ Complete manuscript: 5744/ Number of references: 53/ Number of figures/tables: 5 (including Table of Contents).

ABSTRACT

Melanoma is a malignant proliferative disease originated from melanocyte transformations, which are characterized by a high metastatic rate and mortality. Advances in Nanotechnology have provided useful new approaches and tools for antitumor chemotherapy. The aim of this study was to investigate the molecular mechanisms underlying chitosan nanoparticles containing S-nitroso-mercaptosuccinic acid (S-nitroso-MSA-CS)-induced cytotoxicity in melanoma cells. S-nitroso-MSA-CS induced concentration-dependent cell death against B16-F10 tumor cells, whereas non-nitroso nanoparticles (CS or MSA-CS) did not induce significant cytotoxicity. Additionally, melanoma cells were more sensitive to cell death than normal melanocytes. S-nitroso-MSA-CS-induced cytotoxicity exhibited features of caspase-dependent apoptosis and it was associated with oxidative stress, characterized by increased mitochondrial superoxide production and oxidation of protein thiol groups. In addition, tyrosine nitration and cysteine S-nitrosylation of amino acid residues in cellular proteins were observed. The potential use of these nanoparticles in antitumor chemotherapy of melanoma is discussed.

Keywords: Cytotoxicity, Melanoma, Nanoparticles, Nitric Oxide, S-nitrosothiol.

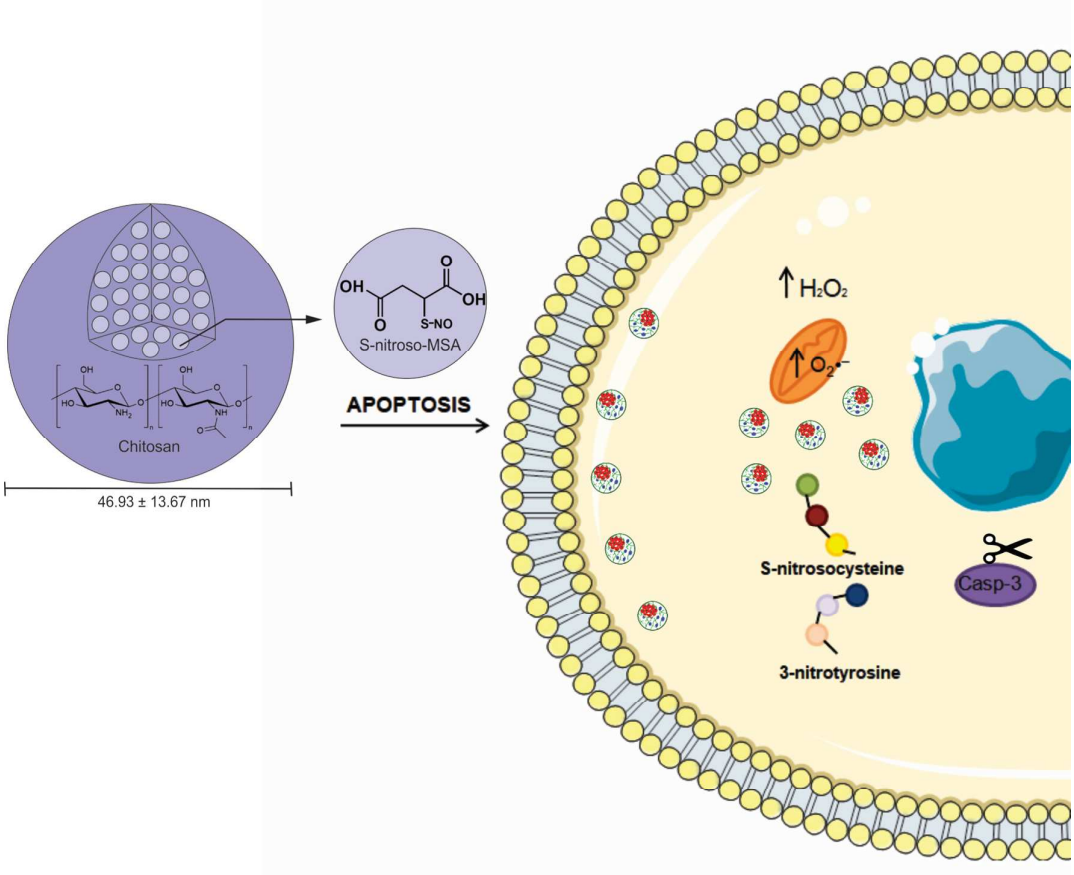

Graphical Table of Contents. Scheme illustrating molecular alterations related to cell death elicited by S-nitroso-MSA-CS nanoparticles in melanoma.

INTRODUCTION

Skin cancer is the most common type of cancer in Caucasian populations,[1] and the clinical classifications are based on the tumor origin and divided into non-melanoma skin cancer and melanoma.[2] Melanoma arises from cumulative abnormalities in melanocytes in response to ultraviolet-induced DNA damage, resulting in genetic mutations that support their malignancy through stimulation of blood vessel growth, evasion of the immune response and apoptosis, tumor invasion and metastasis.[3] Specific gene mutations are associated with an increased risk of melanoma, e.g., the substitution of valine (V) to glutamic acid (E) at position 600 in the BRAF gene (BRAF V600E), which is reported in 40-50% of melanoma cases.[4]

Early diagnosis of melanoma is crucial for the effectiveness of treatment and favorable prognosis of patients. Available tools for melanoma treatment include surgical excision, immunotherapy, radiotherapy, and chemotherapy.[5] Immunotherapy (ipilimumab) or targeted therapy (vemurafenib) are the main chemotherapeutic approaches used for the treatment of metastatic melanoma when the BRAF V600E mutation is expressed.[6] Antitumor drugs have serious side effects, including hypotension, neutropenia, gastrointestinal and skin dysfunctions, and hair loss.[6] Specifically, for the treatment of melanoma, toxic side effects described for vemurafenib include photosensitivity, follicular hyperkeratosis, maculopapular rash, arthralgia, QT prolongation, and others.[7] For ipilimumab, the most common side effects described include diarrhea, nausea, constipation, abdominal pain, vomiting, vitiligo and dermatitis,[8] although more deleterious side effects had already been described such as hepatitis,[9] enterocolitis,[10] pancreatitis and nephritis.[11] New approaches are emerging in the drug discovery field due to the recent advances in Nanotechnology, providing additional opportunities to overcome drug resistance and toxicity, which are considered the major limitations in melanoma chemotherapy.[12] These nanotechnological strategies involve the development of several types of nanostructured drug delivery systems focused on the

improvement of the specificity and efficacy of chemotherapeutic drugs, increasing the drug concentration inside the tumor mass, and decreasing toxicity of chemotherapy.[13]

Polymeric nanoparticles form colloidal systems, which are potentially useful for carrying drugs with low water solubility and/or controlling drug release, providing increased stability and drug delivery profile.[14] Therefore, chitosan, which is a biocompatible, nontoxic, and biodegradable polymer with pharmaceutical applications, has been widely used for nanoparticle preparation.[15] It is well known that nitric oxide (•NO) is involved in various physiological cellular processes such as differentiation and apoptosis.[16] At high concentrations, •NO exhibit anticancer properties;[17] however, due to its short half-life in biological environments (1-5 s), it becomes difficult to reach these antitumor concentrations.[18] To increase their bioavailability and *in vivo* stability, low molecular weight molecules capable of acting as •NO donors, such as S-nitrosothiols (RSNOs), have been developed.[19] Considering that •NO-releasing polymeric nanomaterials are emerging as a promising strategy in cancer chemotherapy,[20] biocompatible chitosan nanoparticles (CS) were synthesized and used to encapsulate low molecular weight mercaptosuccinic acid (MSA), a thiol-containing small molecule. Free thiol groups on mercaptosuccinic chitosan nanoparticles (MSA-CS) were nitrosated to form S-nitroso-MSA-containing chitosan nanoparticles (S-nitroso-MSA-CS). S-nitroso-MSA belongs to the class of RSNOs and acts as a •NO donor. S-nitroso-MSA-CS was previously synthesized and characterized and had its cytotoxicity screened in different cancer cells lines.[21] Additionally, the transdermal •NO delivery in human skin upon dermatological application of S-nitroso-MSA-CS was demonstrated.[22] Here, we investigated the underlying mechanisms of cytotoxicity of S-nitroso-MSA-CS in an *in vitro* melanoma model.

EXPERIMENTAL SECTION

Synthesis of MSA-CS and nitrosation to produce S-nitroso-MSA-CS

CS nanoparticles were prepared using an ionotropic gelation process.[23] Briefly, 0.1 g of CS was solubilized in 0.1 L of 1% acetic acid plus 66.7 mM MSA. Under magnetic stirring, 5.0 mL of 0.6 mg/mL sodium tripolyphosphate was added dropwise in 15 mL of MSA-CS suspension. The final mixture was stirred for 45 minutes at 25°C to form the aqueous suspension of CS (1.0 mg/L of CS) containing 7.5 mg/mL of MSA (which corresponds to 50 mM MSA). Control CS was prepared without the addition of MSA. The thiol groups of MSA-CS were nitrosated by reacting with an equimolar amount of sodium nitrite in acidified medium, as previous described.[24] This solution was homogenized, protected from light, incubated for 30 min, and used immediately in experiments. The formation of S-nitroso-MSA-CS was confirmed by the detection of S-NO characteristic absorption bands at 336 and 545 nm.

Cell culture and standard incubation conditions with NPs

Cell line B16-F10 was purchased from the Rio de Janeiro Cell Bank (BCRJ 0046) (murine melanoma), and Melan-A (murine normal melanocytes) was generously provided by Prof. Miriam Galvonas Jasiulionis (UNIFESP) in 2015. Consequently, the authors performed no additional authentication. All cell lines were tested to be mycoplasma-free by indirect staining with Hoechst 33258 (Thermo Fisher Scientific, USA) and were used within 3 months of thawing the frozen stock. Cells were grown in DMEM (Dulbecco's Modified Eagle's medium) high glucose medium (Sigma-Aldrich, USA) pH 7.2, supplemented with 10% fetal bovine serum (Gibco, Invitrogen, USA), 100 U/mL penicillin and 100 μg/mL streptomycin, in a 5% CO_2 atmosphere at 37°C (Panasonic MCO-19AIC, Japan). For experiments, cells were

detached, centrifuged (160×*g* for 10 minutes), and suspended in supplemented DMEM medium. B16-F10 cells (5.26×10^4 cells/cm^2) were added to microplates for 24 h for cell adhesion. After, S-nitroso-MSA-CS (20 and 40 μg/mL) was added and incubated for additional 24 h.

Cytotoxicity assays

The cytotoxicity of NPs was screened by the trypan blue dye exclusion assay in B16-F10 melanoma cells and melanocytes Melan-A. Compounds were added at increasing concentrations (5.0, 10, 20, and 40 μg/mL) and incubated for 24 h. After this, trypan blue was added 0.016% (w/v) and cells were counted using a Neubauer chamber. Additionally, the effects of modulators of cell death induced by S-nitroso-MSA-CS were evaluated by the MTT reduction test. Thus, after an incubation period, 0.25 mg/mL MTT was added and incubated for 4 h. Then, 0.1 mL of 10% SDS was added, incubated overnight, and plates were read at 570 nm/620 nm (Biochrom Asys Expert Plus Microplate Reader, Biochrom Ltd., UK). The modulators [50 μM Boc-D-FMK (Sigma-Aldrich, USA), 5 μM MY5445 (Tocris Bioscience, USA), 100 μM PTIO (Sigma-Aldrich, USA)] were pre-incubated 1 hour before the addition of the nanoparticles. Cell viability in both assays was calculated in relation to the control (absence of NPs), which was considered as 100%.

Lactate dehydrogenase (LDH) release

After a standard incubation, cells were detached and centrifuged (160×*g* for 10 minutes) and supernatants were kept at 4°C. LDH activity released by cells was determined through NADH oxidation measured using the LDH assay kit according to the manufacturer instructions (Labtest Diagnostica SA, Brazil). Triton X-100 (0.2%) was used as positive control.

Annexin V-FITC/PI double staining flow cytometry analysis

After a standard incubation, cells were detached, centrifuged (160×*g* for 10 minutes) and suspended in 50 µL of binding buffer[25] plus 5.0 µL Annexin V-FITC (BD Biosciences, USA) and 5.0 µL PI (BD Biosciences, USA). The mixture was incubated in the dark at room temperature for 20 minutes. After addition of 0.3 mL of binding buffer, fluorescence emission was measured with a FACSCanto II Flow Cytometer (BD Biosciences), acquiring 10,000 events per sample using a Coherent® Sapphire™ 488-20 solid state blue laser with an excitation at 488 nm, dichroic mirror 502 LP, bandpass filter 530/30 for the FITC fluorescence channel and dichroic mirror 556 LP, bandpass filter 585/42 for the PI fluorescence channel. Data analysis and graphs was completed using Flow Jo vX.0.7 software (Ashland, USA).

Active caspase 3

Caspase 3 was measured by flow cytometry using a monoclonal antibody against the active form. After a standard incubation, cells were fixed with 2% paraformaldehyde in PBS for 30 min and permeabilized with 0.01% saponin in PBS for 15 min at room temperature. Cells were then collected and incubated with 10 µL anti-active-caspase-3 monoclonal antibody conjugated with FITC #559565 (BD-Pharmingen, USA). After a 40-min incubation at 37 °C, the fluorescence emission was analyzed acquiring 10,000 events per sample using blue laser excitation (488 nm), dichroic mirror 502 LP, bandpass filter 530/30 and the FITC fluorescence channel with a FACSCanto II Flow Cytometer. Data analysis and graphs were completed using Flow Jo vX.0.7 software.

Reduced protein thiol content

Total protein –SH groups were quantified using 5,5′-dithiobis (2-nitrobenzoic) acid (DTNB). After a standard incubation, cells were detached and centrifuged for 10 min at 700×g. The pellet was treated with 0.2 ml of 6% trichloroacetic acid and centrifuged at 6000×g for 15 min to precipitate the proteins. This precipitate was suspended with 1 ml of 0.5 M potassium phosphate buffer pH 7.6 by vortexing. After the addition of 0.1 mM DTNB, absorbance was determined at 412 nm (UV-Visible Spectrophotometer UV-1800, Shimadzu, Japan).

Reactive oxygen species (ROS) production

After a standard incubation, cells were collected and loaded with 5 µM MitoSOX™ Red or 5 µM CM-H_2DCFDA (Life Technologies, Invitrogen, USA) for 30 minutes. As positive controls, 20 µM antimycin A and 100 µM hydrogen peroxide (H_2O_2) were used. End time fluorescence emission was measured using the blue laser with an excitation at 488 nm, dichroic mirror 502 LP, bandpass filter, 530/30 FITC fluorescence channel for CM-H_2DCFDA and the dichroic mirror 556 LP, bandpass filter 585/42 for the PI fluorescence channel for MitoSOX™ Red with a FACSCanto II Flow Cytometer. Data analysis and graphs was completed using Flow Jo vX.0.7 software. Alternatively, continuous ROS production was evaluated. After incubation with S-nitroso-MSA-CS for 2 h, cells were loaded with 5 µM CM-H_2DCFDA for 30 min and fluorescence was kinetically recorded for 120 minutes in a microplate reader Synergy HT (Biotek Instruments, USA) at 485 nm and 528 nm excitation and emission, respectively. As positive control, 2 mM *t*-BOOH (Sigma-Aldrich, USA) was used, and 100 U/mL PEGylated catalase (Sigma-Aldrich, USA) was used to distinguish the fluorescence signal attributed exclusively to the peroxide production.

Detection of cysteine S-nitrosylation and tyrosine 3-nitration

After a standard incubation, cells were fixed with 2% paraformaldehyde in PBS for 30 min and permeabilized with 0.01% saponin in PBS for 15 min at room temperature. Cells were then incubated overnight with the rabbit polyclonal anti-nitrotyrosine primary antibody (#9691, Cell Signaling, USA) (1:200) and mouse monoclonal S-nitrosocysteine primary antibody (#ab94930, Abcam, UK) (1:200). After, secondary antibodies – goat anti-Rabbit IgG (H+L) with Alexa Fluor 488 (#A11034, Cell Signaling, USA) (1:500) or goat Anti-Mouse IgG with FITC (#F8521, Sigma-Aldrich, USA) (1:500) – were incubated for one hour at room temperature. Nuclei were stained with 5 nM SlowFade® Gold Antifade Mountant with DAPI (Thermo Fisher Scientific, USA) for 15 min. Fluorescence emissions were acquired with a widefield fluorescence microscopy system Leica AF6000 (Leica Microsystems, Germany) using the set of cube filters A4 (Ex: 360/40, dichroic mirror: 400 nm: Filter BP: 470/40) and L5 (Ex: 480/40; dichroic mirror: 505 nm; BP filter: 527/30), objective lens HCX APO U-V-I 100 x/1.3 OIL, and camera DFC365FX.

Statistical analyses

Values were obtained from at least three independent experiments run in triplicate. Data were expressed as the mean ± SEM, and statistical analyses were performed by a one-way analysis of variance (followed by a Tukey *post hoc* test) with significance defined as *$p<0.05$, **$p<0.01$, *** $p<0.001$.

RESULTS

Enhanced and selective cytotoxicity of S-nitroso-MSA-CS in melanoma B16-F10 cells

The effects of S-nitroso-mercaptosuccinic acid containing chitosan nanoparticles (S-nitroso-MSA-CS) (Fig. 1A) on B16-F10 and Melan-A cell viability were screened by the trypan blue exclusion assay. S-nitroso-MSA-CS exhibited high cytotoxicity against the B16-F10 tumor cell line in a concentration-dependent manner after 24 h of incubation. Such cytotoxicity was higher in tumor cells than in normal melanocytes (Fig. 1B). Additionally, non-nitroso MSA chitosan nanoparticles (MSA-CS), empty chitosan nanoparticles (CS), free S-nitroso-MSA, and MSA (in the same molar ratio used in Fig. 1B) were evaluated in B16-F10 cells and no significant cytotoxicity was achieved, showing the dependence of the nanoparticle structure (Fig. 1c). In flow cytometry, the frontal dispersion of the laser (forward scatter, FSC) gives information about the relative cell size and the lateral dispersion (side scatter, SSC) is related to granularity or complexity of the cell. S-nitroso-MSA-CS decreased cell size and increased the granularity of melanoma cells, defining a ‘dead’ population (Fig. 1D), which was dependent on concentration (Fig. 1E). Additionally, S-nitroso-MSA-CS induced the loss of normal morphology, membrane blebbing, cell shrinkage, emission of plasma membrane projections, and disruption. The loss of adhesion with the external matrix and neighboring cells was also observed (Fig. 1F).

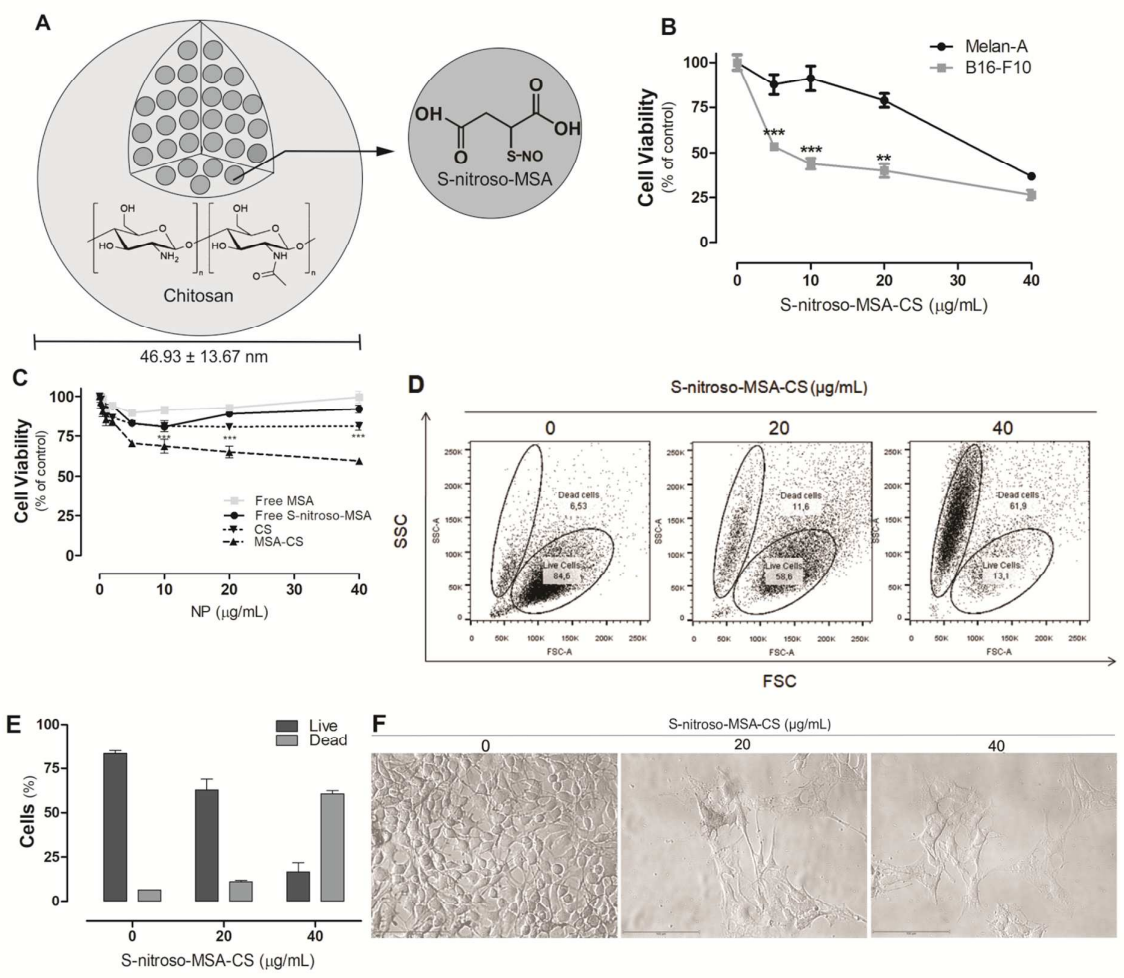

Fig. 1. Enhanced and selective cytotoxicity of S-nitroso-MSA-CS in melanoma B16-F10 cells. (A) Schematic representation of the S-nitroso-MSA-CS nanoparticle structure. **(B)** Effects of S-nitroso-MSA-CS on B16-F10 (gray line) and Melan-A (black line) cell viability assessed by trypan blue assay. ***($p<0.001$) and **($p<0.01$) indicates a difference from Melan-A at each concentration. The results presented as the mean ± SEM of at least three independent experiments performed in triplicate. **(C)** Effects of MSA-CS (dashed line), CS (dotted line), free S-nitroso-MSA (black line), and free MSA (gray line) on B16-F10 cell viability. The results presented as the mean ± SEM of at least three independent experiments performed in triplicate. **(D)** Changes in cell size and granularity (FSC x SSC parameters). Representative dot plots of at least three independent experiments performed in duplicate. **(E)**

Quantification of live and dead cells based on FSC and SSC parameters. The results presented as the mean ± SEM of at least three independent experiments performed in triplicate. **(F)** Morphological alterations of B16-F10 cells assessed by optical microscopy (400× magnification, scale bar 100 μm). Representative images of at least two independent experiments performed in duplicate.

S-nitroso-MSA-CS induced apoptosis in melanoma cells

To obtain a better understanding of S-nitroso-MSA-CS-induced cell death, molecular markers of apoptosis and necrosis were evaluated. Annexin V-FITC/PI double staining flow cytometry revealed the predominance of double stained B16-F10 cells (annexin V^+/PI^+), indicative of late apoptosis (Fig. 2A). Since the dot plot graph is one representative experiment, the quantification of apoptotic cells (annexin V^+), considering all replicates was presented (Fig. 2B). Additionally, the activation of effector caspase 3 during S-nitroso-MSA-CS-induced cell death was shown (Fig. 2C and 2D). The cell-permeable irreversible general caspase inhibitor Boc-D-FMK also prevented cell death (Fig. 2E), corroborating the participation of caspases. The pre-incubation of B16-F10 cells with necrostatin-1 (Sigma-Aldrich #N9037) and IM-54 (Sigma-Aldrich #SLM0412), inhibitors of necroptosis and necrosis, respectively, did not prevent the S-nitroso-MSA-CS-induced cytotoxicity (Fig. 2F and 2G). In accordance, loss of plasma membrane integrity induced by S-nitroso-MSA-CS was not observed, as evaluated through the absence of LDH release by the cells (Fig. 2H). Thus, S-nitroso-MSA-CS induced caspase-dependent apoptosis in melanoma cells.

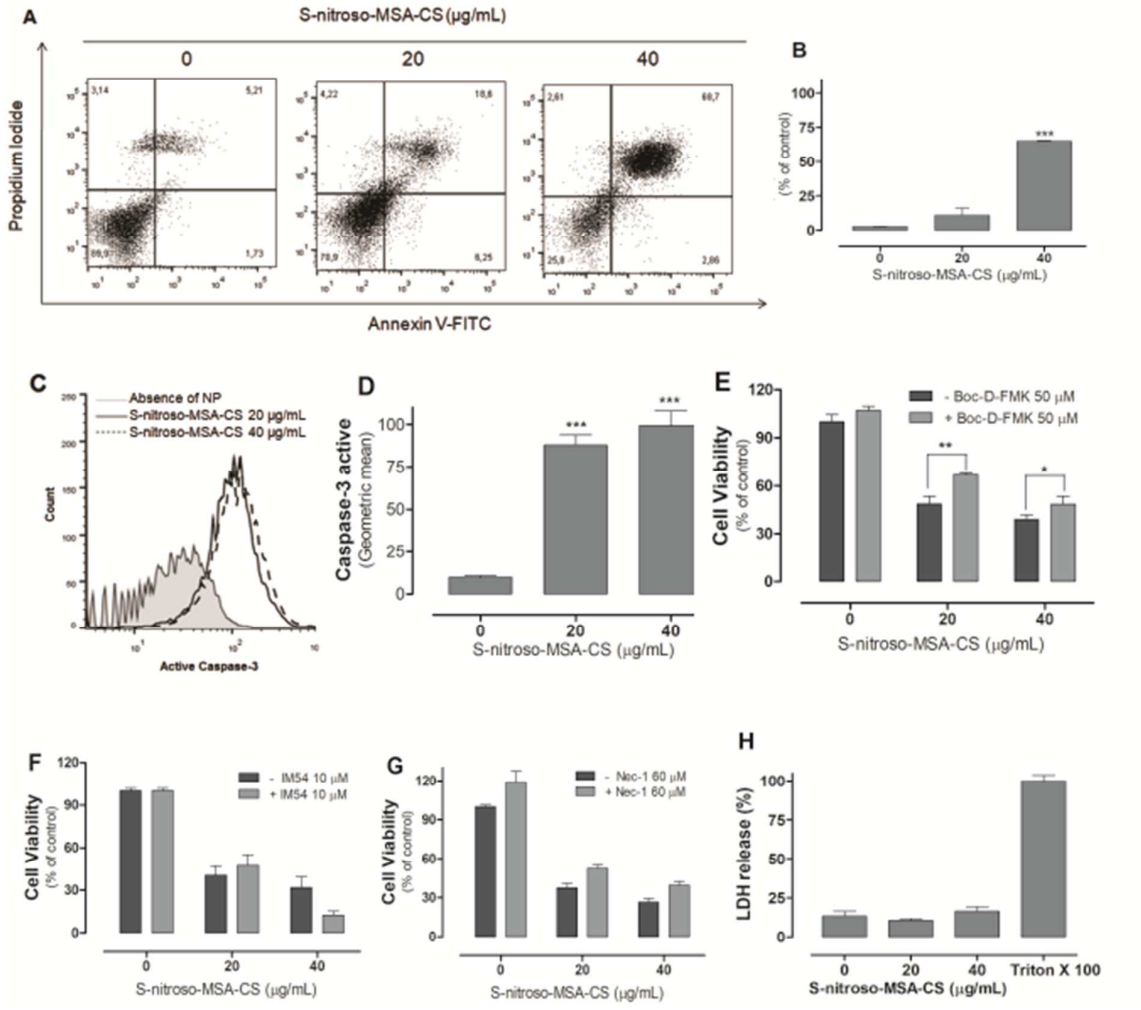

Fig. 2. S-nitroso-MSA-CS induced apoptosis in B16-F10 melanoma cells. (A) Cell death profile achieved by annexin V-FITC/PI double staining flow cytometry analysis. Representative dot plot of at least three independent experiments performed in duplicate. **(B)** Quantification of apoptotic (annexin V-FITC positive) cells. The results presented as the mean ± SEM of at least three independent experiments performed in duplicate. ***($p<0.001$) indicates a difference from control (absence of NPs). **(C)** Activation of caspase-3. Gray line (absence of NPs), black line (S-nitroso-MSA-CS 20 µg/mL), dashed black line (S-nitroso-MSA-CS 40 µg/mL). Representative histogram of at least three independent experiments performed in duplicate. **(D)** Quantification of active caspase 3. Results presented as the mean ± SEM of at least three independent experiments performed in duplicate. ***($p<0.001$)

indicates a difference from control (absence of NPs). Effect of caspase inhibitors on the S-nitroso-MSA-CS-induced cytotoxicity: 50 μM Boc-D-FMK **(E)**, 10 μM IM-54 **(F)**, and 60 μM necrostatin-1 **(G)**. Results presented as the mean ± SEM of at least three independent experiments performed in triplicate. Statistical differences are indicated. **(H)** Estimation of LDH released. LDH activity in control (absence of NPs) was 137.61 ± 32.38 (U/L) and in Triton X-100 was 1036.15 ± 40.47 (U/L). The results presented as the mean ± SEM of at least three independent experiments performed in triplicate.

Increased oxidative stress induced by S-nitroso-MSA-CS

A general view of the cellular reactive oxygen species (ROS) production can be achieved by the assessment of oxidized dichlorofluorescein (DCF) fluorescence emission.[26] Thus, B16-F10 melanoma cells were incubated with S-nitroso-MSA-CS for 24 h and loaded with CM-H_2DCFDA. As observed in Fig. 3A, S-nitroso-MSA-CS at 20 and 40 μg/mL (dashed and black lines, respectively) increased ROS generation in B16-F10 melanoma cells. Hydrogen peroxide (H_2O_2) was used as a positive control (dotted line). The fluorescence quantification of replicates is presented in Fig. 3B. Considering the relative lack of specificity of this fluorophore to identify a specific free radical type, a kinetic measurement of ROS production elicited by S-nitroso-MSA-CS (dashed lines) with CM-H_2DCFDA was performed for 120 minutes in the presence of catalase conjugated with polyethylene glycol (PEG-CAT, solid lines) (Fig. 3C). The quantification of DCF fluorescence emission at 120 minutes revealed that part of the DCF oxidation at 20 μg/mL S-nitroso-MSA-CS was attributed to the peroxide production but at 40 μg/mL S-nitroso-MSA-CS PEG-CAT did not suppress the emission of fluorescence (Fig. 3D), indicating that the radical production profile is different depending on the NPs concentration. Since H_2O_2 can be formed by dismutation of superoxide anions produced by mitochondria, we also evaluated the mitochondrial superoxide generation after a 24 h incubation with NPs using MitoSOX™ Red. As expected, S-nitroso-MSA-CS also

increased the generation of superoxide anion radicals by mitochondria in a concentration dependent fashion (Fig. 3E and 3F). Antimycin A, an inhibitor of the mitochondrial respiratory complex III[27] was used as positive control (Fig. 3E, dotted line). This increased radical production induced by S-nitroso-MSA-CS was accompanied by oxidation of the thiol group of proteins (Fig. 3G).

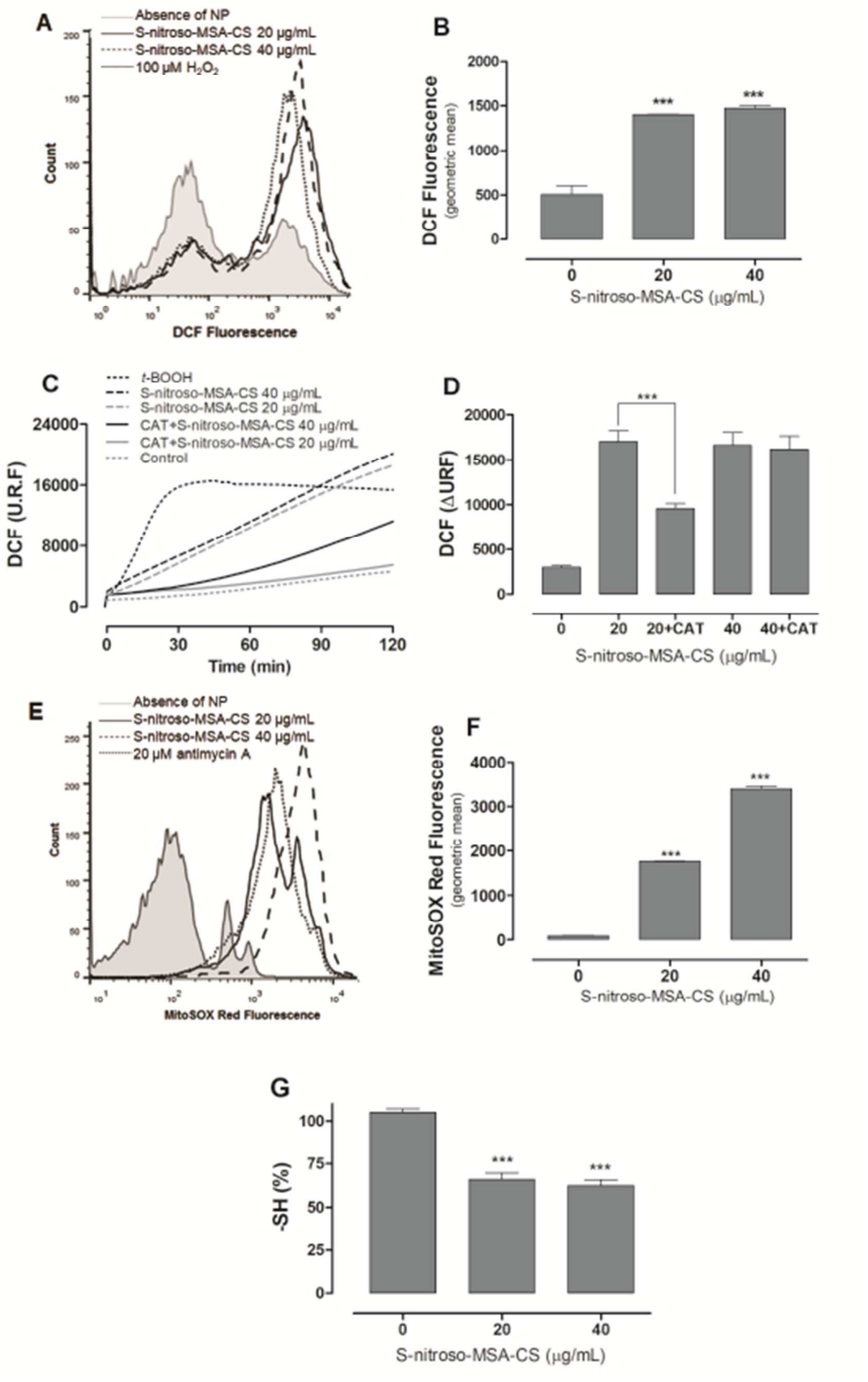
A
Absence of NP
S-nitroso-MSA-CS 20 µg/mL
S-nitroso-MSA-CS 40 µg/mL
100 µM H_2O_2
Count
DCF Fluorescence
B
DCF Fluorescence
(geometric mean)
***
***
S-nitroso-MSA-CS (µg/mL)
C
t-BOOH
S-nitroso-MSA-CS 40 µg/mL
S-nitroso-MSA-CS 20 µg/mL
CAT+S-nitroso-MSA-CS 40 µg/mL
CAT+S-nitroso-MSA-CS 20 µg/mL
Control
DCF (U.R.F)
Time (min)
D
DCF (ΔURF)
***
0
20
20+CAT
40
40+CAT
S-nitroso-MSA-CS (µg/mL)
E
Absence of NP
S-nitroso-MSA-CS 20 µg/mL
S-nitroso-MSA-CS 40 µg/mL
20 µM antimycin A
Count
MitoSOX Red Fluorescence
F
MitoSOX Red Fluorescence
(geometric mean)
***
***
S-nitroso-MSA-CS (µg/mL)
G
-SH (%)
***
***
S-nitroso-MSA-CS (µg/mL)

Fig. 3. Oxidative stress in B16-F10 melanoma cells exposed to S-nitroso-MSA-CS. (A) Representative Histograms of DCF fluorescence obtained by flow cytometry. Gray line (absence of NPs), dotted black line (100 μM H_2O_2), black line (S-nitroso-MSA-CS 20 μg/mL), dashed black line (S-nitroso-MSA-CS 40 μg/mL). **(B)** Quantification of DCF fluorescence considering replicates. The results presented as the mean ± SEM of at least three independent experiments performed in duplicate. ***($p<0.001$) indicates a difference from control (absence of NPs). **(C)** Kinetic measurement of DCF fluorescence. Representative plot of DCFDA fluorescence intensity read at 120 minutes of at least two independent experiments performed in triplicate. **(D)** Quantification of DCF fluorescence from kinetics at t=120 minutes. ***($p<0.001$) indicates a difference from control (absence of NPs). The results presented as the mean ± SEM of at least two independent experiments performed in triplicate. **(E)** Representative histogramS of MitoSOX Red fluorescence obtained by flow cytometry. Gray line (absence of NPs), dotted black line (20 μM antimycin A), black line (S-nitroso-MSA-CS 20 μg/mL), dashed black line (S-nitroso-MSA-CS 40 μg/mL). **(F)** Quantification of MitoSOX Red fluorescence considering replicates. The results presented as the mean ± SEM of at least three independent experiments performed in duplicate. ***($p<0.001$) indicates a difference from control (absence of NPs). **(G)** Reduced thiol content in cellular proteins. The results presented as the mean ± SEM of at least three independent experiments performed in triplicate. ***Different from control (absence of NPs) in panels B, F, and G.

Cysteine S-nitrosylation and tyrosine nitration promoted by S-nitroso-MSA-CS

The incubation of B16-F10 melanoma cells with S-nitroso-MSA-CS (20 and 40 μg/mL) resulted in an increased formation of 3-nitrotyrosine (Fig. 4A) and S-nitrosocysteine (Fig. 4B) in a concentration dependent manner. To evaluate whether these observed effects were due to •NO released by S-nitroso-MSA-CS, cells were pretreated with the •NO scavenger PTIO (Fig. 4C) and with an inhibitor of cyclic GMP phosphodiesterase MY5445 (Fig. 4D). Both

modulators were not able to change the cytotoxicity exerted by S-nitroso-MSA-CS, which provided strong evidence that the protein modifications were not promoted by free cytosolic $^{\bullet}$NO released from the nanoparticles.

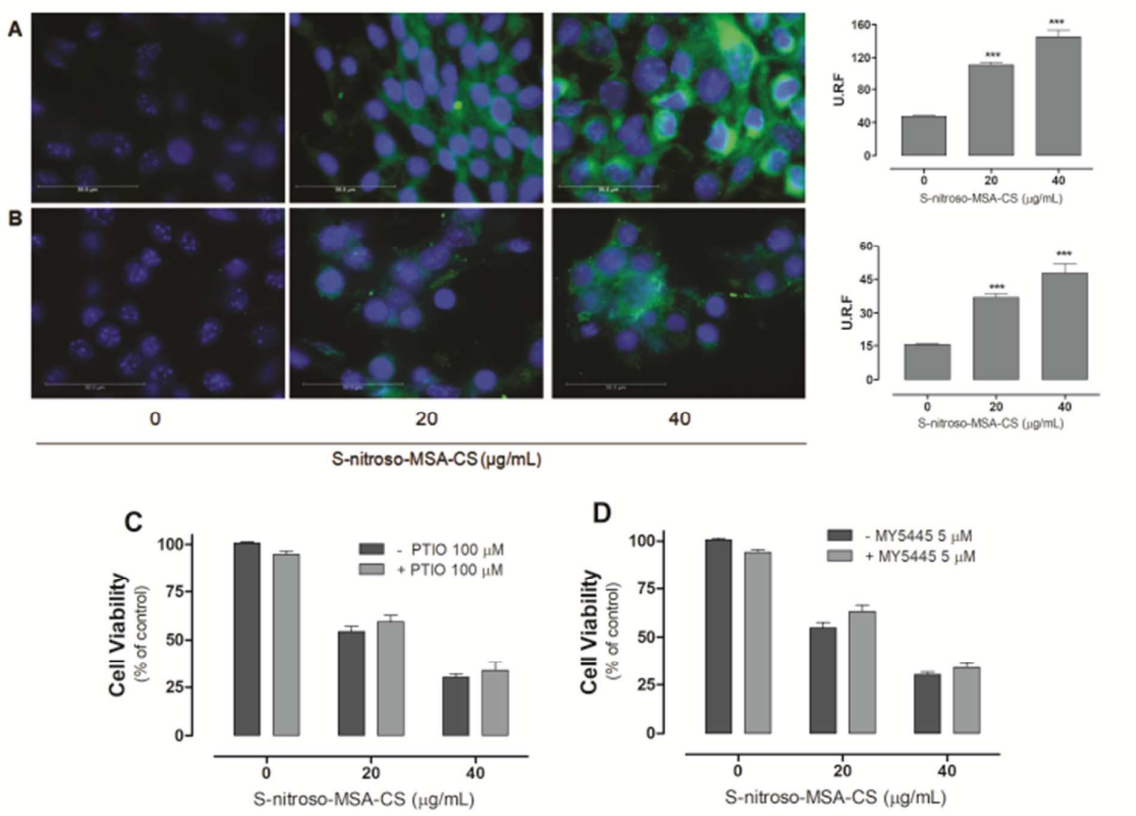

Fig. 4. S-nitrosylation and tyrosine nitration of cellular proteins promoted by S-nitroso-MSA-CS. Indirect immunofluorescence with anti-nitrotyrosine **(A)** and anti-S-nitrosocysteine antibodies **(B)**, with the respective quantification of fluorescence presented on right. Magnification 1000×, scale bars 50 μm. ***($p<0.001$) indicates a difference from control (absence of NPs). Effects of 100 μM PTIO **(C)** and 5 μM MY5445 **(D)** on the S-nitroso-MSA-CS induced cytotoxicity. The results presented as the mean ± SEM of at least three independent experiments performed in triplicate.

DISCUSSION

The cytotoxicity of •NO donors was described in different tumor cell lines, including ovarian cancer,[28,29] lung carcinoma,[30] breast adenocarcinoma,[31] hepatocellular carcinoma[32] neuroblastoma[33] and squamous cell carcinoma of the head and neck.[34] Such effects were associated with the inhibition of cell proliferation and induction of apoptosis.[35] In B16-F10 melanoma cells, organic nitrate •NO donors inhibited their metastatic potential, and DETA/NO •NO donors reversed the resistance to chemotherapeutic agents, including doxorubicin.[36] Additionally, organic nitrate •NO donors prevented the formation of melanoma cell lung nodes in a murine melanoma *in vivo* model.[37] These reports suggest the therapeutic potential use of •NO donor nanomaterials in many types of cancer antitumor chemotherapy, including melanoma. Here, a nanostructured system containing •NO and S-nitroso-MSA-CS exhibited cytotoxicity against B16-F10 melanoma cells with no significant cytotoxicity in normal melanocytes.

The mechanisms of cell death elicited by •NO donors depend on several factors, such as cell type and tumor stage. Sustained •NO production could act as a pro-apoptotic signal by activating caspases[38] through its effect on mitochondria[39,40] or by upregulation of death receptor expression and their sensitization to death ligands, as Fas-L (Fas ligand), TRAIL (tumor necrosis factor–related apoptosis-inducing ligand) and TNF-α (tumor necrosis factor-α).[41] Our data demonstrated that the cytotoxicity induced by S-nitroso-MSA-CS in melanoma cells is through caspase-dependent apoptosis.

It is well established that •NO stimulates the soluble guanylyl cyclase resulting in an increase of intracellular cGMP,[42] whereas cGMP phosphodiesterase leads to a decrease.[43] The cGMP phosphodiesterase inhibitor, MY-5445, increases the intracellular cGMP levels and thus mimics the •NO effect,[44] but it did not alter the cytotoxicity of S-nitroso-MSA-CS, as well as the •NO scavenger PTIO, despite the detection of NO-protein adducts as discussed

below. These data suggest that these nanoparticles probably do not act as a •NO releasing prodrug.

Reactions between •NO and –SH groups of protein cysteine residues lead to S-nitrosylation, which is an important and reversible post-translational modification able to regulate the activity and function of many proteins and cellular processes.[45] S-nitroso-MSA-CS increased cysteine S-nitrosylation and tyrosine nitration in melanoma cells. Probably the S-nitroso groups of S-nitroso-MSA-CS were transferred directly to free thiol groups of proteins through S-(trans)nitrosylation. In agreement, the occurrence of S-(trans)nitrosylation without release of free •NO by RSNOs was previously proposed.[46]

It is well known that the oxidation of protein thiol groups in mitochondrial membranes is related to mitochondrial permeabilization and release of pro-apoptotic proteins to the cytosol, triggering cell death.[47,48] S-nitrosylation induced by S-nitroso-MSA-CS in melanoma cells was accompanied by oxidative stress characterized by H_2O_2 and mitochondrial superoxide overproduction, and by nitration of cellular proteins. In this regard, mitochondrial dysfunctions elicited by •NO donors associated with increased superoxide production have been described.[49] Additionally, ruthenium nitrosyl complexes inhibited mitochondrial respiration in hepatocarcinoma cells, resulting in ATP depletion, ROS production, and cell death.[50] Increased superoxide production in mitochondria may occur due to nitration and inactivation of manganese-dependent superoxide dismutase[51] and/or inhibition of the respiratory chain.[52] These superoxide can react with •NO generating peroxynitrite that nitrates –OH groups in tyrosine residues irreversibly, and the adduct 3-nitrotyrosine is widely used as a nitrosative stress marker.[53]

In summary, we presented here the cytotoxic effects of S-nitroso-MSA-CS on B16-F10 melanoma cells. Such effects were selective to tumor cells when compared to normal melanocytes and dependent on the entire nanoparticle composition; only CS, free MSA or

free S-nitroso-MSA did not exhibit significant cytotoxicity. Additionally, the investigation of molecular mechanisms of cytotoxicity revealed that S-nitroso-MSA-CS induced an apoptotic cell death profile, dependent on caspase activation, and associated with a cellular and mitochondrial oxidative stress. Together these results point to the potential use of S-nitroso-MSA-CS as an antitumor chemotherapy of melanoma.

DISCLOSURE OF POTENTIAL CONFLICTS OF INTEREST

The other authors disclosed no potential conflicts of interest.

ACKNOWLEDGMENTS

Melan-A cells were kindly provided by Prof. Miriam Galvonas Jasiulionis from the Federal University of São Paulo (Unifesp). This work was supported by Brazilian funding agencies FAPESP (2012/12247-8; 2016/07367-5) and CNPq (486760/2013-0). CAPES provided the scholarship to Leticia Silva Ferraz.

REFERENCES

[1] Byrd-Miles, K.; Toombs, E.L.; Peck, G.L. Skin cancer in individuals of African, Asian, Latin–American, and American–Indian descent: differences in incidence, clinical presentation, and survival compared to Caucasians. *J Drugs Dermatol* **2007**, 6, 10-16.

[2] Haque, T.; Rahman, K.M.; Thurston, D.E.; Hadgraft, J.; Lane, M.E. Topical therapies for skin cancer and actinic keratosis. *Eur J Pharm Sci* **2015**, 77, 279-289.

[3] Ibrahim, S.F.; Brown, M.D. Actinic keratoses: a comprehensive update. *Am J Clin Dermatol* **2009**, 2, 43–48.

[4] Thompson, J.F.; Scolyer, R.A.; Kefford, R.F. Cutaneous melanoma. *Lancet* **2015**, 365, 687-701.

[5] Ridnour, L.A.; Thomas, D.D.; Switzer, C. Molecular mechanisms for discrete nitric oxide levels in cancer. *Nitric Oxide* **2008**, 19, 73-76.

[6] Chapman, P.B.; Hauschild, A.; Robert, C.; Haanesn, J.B.; Ascierto, P.; Larkin, J.; Dummer, R.; Garbe, C.; Testori, A.; Maio, M. *et al.* Improved survival with vemurafenib in melanoma with BRAF V600E mutation. *N Engl J Med* **2011**, 364, 2507-2516.

[7] Hagen, B.; Trinh, V.A. Managing Side Effects of Vemurafenib Therapy for Advanced Melanoma. *J Adv Pract Oncol* **2014**, 5, 400-410.

[8] Mansh, M. Ipilimumab and Cancer Immunotherapy: A New Hope for Advanced Stage Melanoma. *Yale J Biol Med* **2011**, 84, 381-389.

[9] Chmiel, K.D.; Suan, D.; Liddle, C.; Nankivell, B.; Ibrahim, R.; Bautista, C.; Thompson, J.; Fulcher, D.; Kefford, R. Molecular mechanisms for discrete nitric oxide levels in cancer. *J Clin Oncol* **2011**, 29, 237-240.

[10] Minor, D.R.; Chin, K.; Kashani-Saber, M. Infliximab in the treatment of anti-CTLA4 antibody (ipilimumab) induced immune-related colitis. *Cancer Biother Radiopharm* **2009**, 24, 321-325.

[11] Weber J. Ipilimumab: controversies in its development, utility and autoimmune adverse events. *Cancer Immunol Immunother* **2009**, 58, 823-830.

[12] Brys, A.K.; Gowda, R.; Loriaux, D.B.; Robertson, G.P.; Mosca, P.J. Nanotechnology-based strategies for combating toxicity and resistance in melanoma therapy. *Biotechnol Adv* **2016**, 34, 565-577.

[13] Li, J.; Wang, Y.; Liang, R.; An, X.; Wang, K.; Shen, G.; Tu, Y.; Zhu, J.; Tao, J. Recent advances in targeted nanoparticles drug delivery to melanoma. *Nanomedicine* **2015**, 11, 769-794.

[14] Kumari, A.; Sudesh, K.Y.; Subhash, C.Y. Biodegradable polymeric Nanoparticles based drug delivery systems. *Colloids Surf B Biointerfaces* **2010**, 75, 1-18.

[15] Chandra, S. Chakraborty, N.; Dasgupta, A.; Sarkar, J.; Panda, K.; Acharya, K. Chitosan Nanoparticles: A positive modulator of innate immune responses in plants. *Sci Rep* **2015**, 5, 15195.

[16] Saraiva, J.; Marotta-Oliveira, S.S.; Cicillini, A.S.; Eloy, J.O.; Marchetti, J.M. Nanocarriers for Nitric Oxide Delivery. *J drug deliv* **2011**, 2011, 936438.

[17] Ding, Q.G.; Zang, J.; Gao, S.; Gao, Q.; Duan, W., Li, X.; Li, X.; Xu, W.; Zhang, Y. *et al.* Nitric oxide donor hybrid compounds as promising anticancer agents. *Drug Discov Ther* **2017**, 10, 276-284.

[18] Quinn, J.F.; Whittaker, M.R.; Davis, T.P. Delivering nitric oxide with nanoparticles. *J Control Release* **2015**, 205, 190–205.

[19] Seabra, A.B.; Justo, G.Z.; Haddad, P.S. State of the art, challenges and perspectives in the design of nitric oxide-releasing polymeric nanomaterials for biomedical applications. *Biotechnol Adv* **2015**, 1, 1370-1379.

[20] Seabra, A.B.; de Lima, R.; Calderón, M. Nitric oxide releasing nanomaterials for cancer treatment: Current status and perspectives. *Curr Med Chem* **2015**, 15, 298-308.

[21] Pelegrino, M.T.; Silva, L.C.; Watashi, C.M.; Haddad, P.S.; Rodrigues, T.; Seabra, A.B. Nitric oxide-releasing nanoparticles: synthesis, characterization, and cytotoxicity to tumorigenic cells. *J Nanopart Res* **2017**, 19, 57.

[22] Pelegrino, M.T.; Weller, R.; Chen, X.; Bernardes, J.S.; Seabra, A.B. Chitosan nanoparticles for nitric oxide delivery in human skin. *MedChemComm* **2017**, 8, 713-719.

[23] Tripathy, S.; Das, S.; Chakraborty, S.K.; Sahu, S.K.; Pramanik, P.; Roy, S. Synthesis, characterization of chitosan-tripolyphosphate conjugated chloroquine nanoparticle and its in vivo anti-malarial efficacy against rodent parasite: A dose and duration dependent approach. *Int J Pharm* **2012**, 434, 292–305.

[24] Cardozo, V.F.; Lancheros, C.A.; Narciso, A.M.; Valereto, E.C.; Kobayashi, R.K.; Seabra, A.B., Nakazato, G. Evaluation of antibacterial activity of nitric oxide-releasing polymeric particles against *Staphylococcus aureus* from bovine mastitis. *Int J Pharm* **2014**, 473, 20-29.

[25] Moraes, V.W.R.; Caires, A.C.F.; Paredes-Gamero, E.J.; Rodrigues, T. Organopalladium compound 7b targets mitochondrial thiols and induces caspase-dependent apoptosis in human myeloid leukemia cells. *Cell Death Dis* **2013**, 4, e658.09.

[26] Brenner, C.; Moulin, M. Physiological roles of the permeability transition pore. *Circ Res* **2012**, 111: 1237-1247.

[27] Stevens, E.V.; Carpenter, A.W.; Shin, J.H.; Liu, J.; Der, C.J.; Schoenfisch, M.H. Nitric Oxide-Releasing Silica Nanoparticle Inhibition of Ovarian Cancer Cell Growth. *Mol Pharm* **2012**, 7, 775-785.

[28] Kielbik, M.; Szcul-Kielbik, I.; Nowak, M.; Sulowska, Z.; Klink, M. Evaluation of nitric oxide donors impact on cisplatin resistance in various ovarian cancer cell lines. *Toxicol In Vitro* **2016**, 36, 26-37.

[29] Basudhar, D.; Bharadwaj, G.; Cheng, R.Y.; Jain, S.; Shi, S.; Heinecke, J.L.; Holland, R.J.; Ridnour, L.A.; Caceres, V.M.; Spadari-Bratfisch, R.C. *et al.* Synthesis and chemical and biological comparison of nitroxyl- and nitric oxide-releasing diazeniumdiolate-based aspirin derivatives. *J Med Chem* **2013**, 56, 7804-7820.

[30] Basudhar, D.; Cheng, RC, Bharadwaj, G.; Ridnour, L.A.; Wink, D.A.; Miranda, K.M. Chemotherapeutic potential of diazeniumdiolate-based aspirin prodrugs in breast cancer. *Free Radic Biol Med* **2015**, 83, 101-114.

[31] Zhou, L.; Zhang, H.; Wu, J. Effects of nitric oxide on the biological behavior of HepG2 human hepatocellular carcinoma cells. *Exp Ther Med* **2016**, 11, 1875-1880.

[32] Duong, H.T.; Kamarudin, Z.M.; Erlich, R.B.; Li, Y.; Jones, M.W.; Kavallaris, M.; Boyer, C.; Davis, T.P. Intracellular nitric oxide delivery from stable NO-polymeric nanoparticle carriers. *Chem Commun* **2013**, 49, 4190-4192.

[33] Duan, S.; Cais, S.; Yang, Q.; Forrest, M.L. Multi-arm polymeric nanocarrier as a nitric oxide delivery platform for chemotherapy of head and neck squamous cell carcinoma. *Biomaterials* **2012**, 33, 3243-3253.

[34] Vannini, F.; Kashfi, K.; Nath, M. The dual role of iNOS in cancer. *Redox Biol* **2015**, 6, 334-343.

[35] Postovit, L.M.; Adams, M.A.; Lash, G.E.; Heaton, J.P.; Graham, C.H. Nitric oxide-mediated regulation of hypoxia-induced B16F10 melanoma metastasis. *Int J Cancer* **2004**, 108, 47-53.

[36] Matthews, N.E.; Adams, M.A.; Maxwell, L.R.; Gofton, T.E.; Graham, C.H. Nitric oxide-mediated regulation of chemosensitivity in cancer cells. *J Natl Cancer Inst* **2001**, 93, 1879-1885.

[37] Kim, Y.M.; Chung, H.T.; Simmons, R.L.; Billiar, T.R. Cellular non-heme iron content is a determinant of nitric oxide-mediated apoptosis, necrosis, and caspase inhibition. *J Biol Chem* **2000**, 275, 10954-61.

[38] Messmer, U.K.; Ankarcrona, M.; Nicotera, P.; Brune, B. p53 expression in nitric oxide-induced apoptosis. *FEBS Lett* **1994**, 335, 23–26.

[39] Brune, B. Nitric oxide: NO apoptosis or turning it ON? *Cell Death Differ* **2003**, 10, 864-869.

[40] Bonavida, B.; Garban, H. Nitric oxide-mediated sensitization of resistant tumor cells to apoptosis by chemo-immunotherapeutics. *Redox Biol* **2015**, 6, 486-494.

[41] Francis, S.H., Busch, J.L.; Corbin, J.D. cGMP-Dependent Protein Kinases and cGMP Phosphodiesterases in Nitric Oxide and cGMP Action. *Pharmacol Rev* **2010**, 62, 525-563.

[42] Hagiwara, M.; Endo, T.; Kanayama, T.; Hidaka, T. Effect of 1-(3-Chloroanilino)-4-Phenylphthalazine (MY-5445), a Specific Inhibitor of Cyclic GMP Phosphodiesterase, on Human Platelet Aggregation. *J Pharmacol Exp Ther* **1984**, 228, 467-471.

[43] Bonavida, B.; Khineche, S.; Huerta-Yepes, S.; Garbán, H. Therapeutic potential of nitric oxide in cancer. *Drug Resist Upda* **2006**, 9, 157-173.

[44] Miller, M.R.; Megson, I.L. Recent developments in nitric oxide donor drugs. *Br J Pharmacol.* **2007**, 151, 305-321.

[45] Lebel, C.P.; Bondy, S.C. Sensitive and rapid quantization of oxygen reactive species formation in rat synaptosomes. *Neurochem Int* **1990**, 17, 435-40.

[46] Santana, D.P.; de Faria, P.A.; Paredes-Gamero, E.; Caires, A.C.; Nantes, I.L.; Rodrigues, T. Palladacycles catalyse the oxidation of critical thiols of the mitochondrial membrane proteins and lead to mitochondrial permeabilization and cytochrome c release associated with apoptosis. *Biochem J* **2009**, 417, 247-256.

[47] Cruz, T.S.; de Faria, P.A.; Santana, D.P.; Ferreira, J.C.; Oliveira, V.; Nascimento, O.R., Rodrigues, T. On the mechanisms of phenothiazine-induced mitochondrial permeability transition: Thiol oxidation, strict Ca^{2+} dependence, and cyt c release. *Biochem Pharmacol* **2010**, 80,1284-1295.

[48] Boyd, C.S.; Cadenas, E. Nitric Oxide and Cell Signaling Pathways in Mitochondrial-Dependent Apoptosis. *J Biol Chem* **2002**, 383, 411-423.

[49] Pestana, C.R.; Phelippin, D.P.S.; Polizello, A.C.M.; Dorta, D.J.; Uyemura, S.A.; Santos, A.C. Effects on mitochondria of mitochondria-induced nitric oxide release from a ruthenium nitrosyl complex. *Nitric Oxide* **2009**, 20, 24-30.

[50] Macmillan-Crow, L.A.; Crow, J.P.; Kerby, J.D.; Beckman, J.S.; Thompson, J.A. Nitration and inactivation of manganese superoxide dismutase in chronic rejection of human renal allografts. *Proc Natl Acad Sci USA* **1996**, 93, 11853-11858.

[51] Rodrigues, F.P.; Pestana, C.R.; Polizello, A.C.; Pardo-Andreu, G.L.; Uyemura, S.A.; Santos, A.C.; Alberici, L.C.; da Silva, R.S.; Curti, C. Release of NO from a nitrosyl ruthenium complex through oxidation of mitochondrial NADH and effects on mitochondria. *Nitric Oxide* **2012**, 26, 174-181

[52] Murray, J.; Taylor, S.W.; Zhang, B.; Ghosh, S.S.; Capaldi, R.A. Oxidative damage to mitochondrial complex I due to peroxynitrite: identification of reactive tyrosines by mass spectrometry. *J Biol Chem* **2003**, 278, 37223–37230.

[53] Denninger, J.W.; Marletta, M.A. Guanylate cyclase and the NO/cGMP signaling pathway. *Biochim Biophys Acta* **1999**, 1411, 334-350.